Supplementary Information

A Dual-Template MOF/ZIF Approach for Structurally Optimized Metal Oxide@CNT and Porous Carbon Electrodes in Supercapacitors

Tabbu Shaikh[a], Omkar Kulkarni[a], Maheswari Arunachalam[b], Soon Hyung Kang[b], Sanjay Kolekar[a]**

[a]Analytical Chemistry and Materials Science Research Laboratory, Department of Chemistry, Shivaji University, Kolhapur - 416004, India

[b]Department of Chemistry Education and Optoelectronic Convergence Research Centre, Chonnam National University, Gwangju, 61186, Republic of Korea

Corresponding author: skang@jnu.ac.kr; sskolekar@gmail.com

Contents

1. Experimental Section

2. List of Figures and Captions

Fig. S1. (a) EDX spectrum and (b) SAED pattern of the NCM-derived NCO@CNT composite.

Fig. S2. (a) Nitrogen adsorption–desorption isotherms and (b) BJH pore size distribution curves of NCM-derived NCO and NCM-derived NCO@CNT composites.

Fig. S3. (a,b) CV curves of NCM and NCM-derived NCO at scan rates ranging from 10 to 100 mV s^{-1}. (c,d) Galvanostatic charge–discharge (GCD) curves of NCM and NCM-derived NCO at current densities from 1 to 10 mA cm^{-2}.

Fig. S4. (a) Simulated Nyquist plot of NCM-derived NCO@CNT (inset: equivalent circuit). (b) Log(scan rate) versus log(peak current). (c,d) CV curves showing capacitive and diffusion-controlled contributions at 10 mV s^{-1} for NCM-derived NCO and NCM-derived NCO@CNT. (e,f) Percentage contributions of capacitive and diffusion-controlled processes at various scan rates.

Fig. S5. Cycling stability of ZC over 5,000 charge–discharge cycles (inset: comparison of the first and last five cycles).

Fig. S6. Specific capacitance of the NCM-derived NCO@CNT//ZC composite at different current densities.

1. Experimental Section

1.1. Chemicals

Nickel nitrate hexahydrate ($Ni(NO_3)_2.6H_2O$), cobalt nitrate hexahydrate ($Co(NO_3)_2.6H_2O$), N, N-dimethyl formamide (DMF) (C_3H_7ON), zinc nitrate hexahydrate ($Zn(NO_3)_2.6H_2O$), methanol (CH_3OH) and potassium hydroxide (KOH) were received from Loba Chemie. Acetylene black and N-methyl pyrrolidone (NMP) (C_5H_9O) were purchased from Alfa Aesar. 2,5-thiophenedicarboxylic acid ($C_6H_4O_4S$), 2-methylimidazole ($C_4H_6N_2$) and polyvinylidene difluoride (PVDF) $(CH_2CF_2)n$ and CNTs were acquired from Sigma Aldrich. No additional processing was needed, and all the chemicals were used as provided.

1.2. Synthesis of NCM and NCM@CNT

1.2.1. Synthesis of NCM.

NCM was synthesised through a reflux-condensation process. Nickel nitrate hexahydrate (0.1 M), cobalt nitrate hexahydrate (0.1 M), and 2,5-thiophenedicarboxylic acid (0.15 M) were dissolved in dimethylformamide (DMF) to form a homogeneous solution, which was transferred to a 100 mL round-bottom flask. The mixture was refluxed at 120 °C for 12 h. After cooling to room temperature, the resulting purple precipitate was collected by filtration, washed thoroughly with DMF and ethanol, and dried in a vacuum oven at 60 °C for 12 h.

1.2.2. Synthesis of NCM@CNT.

NCM@CNT was prepared following the same procedure described above, with the addition of 2 mL of a CNT suspension (1 mg mL^{-1}) to the precursor solution prior to reflux. The incorporation of CNTs during synthesis ensures their uniform integration within the final NCM framework.

1.3. Synthesis NCM-derived NCO and NCM-derived NCO@CNT

NCM and NCM@CNT powders were converted into their corresponding metal oxides through controlled thermal treatment. The materials were placed in a muffle furnace and heated in air at 400 °C for 2 h, yielding NCM-derived NCO and NCM-derived NCO@CNT, respectively. A schematic representation of the overall synthesis process is provided in Fig. 1. (main manuscript).

1.4. Synthesis of ZC as a Negative Electrode

ZIF-8 was synthesized following a previously reported procedure.[1] Zinc nitrate hexahydrate (1.45 g) was dissolved in 50 mL of methanol, while 2-methylimidazole (3.28 g) was dissolved separately in another 50 mL of methanol. Two solutions were combined and stirred for 2 h, after which the mixture was aged at 25 °C for 12 h. The resulting white precipitate was collected by centrifugation, washed several times with ethanol, and dried at 60 °C overnight. To obtain ZIF-derived carbon (ZC), the dried ZIF-8 powder was carbonized at 900 °C for 3 h under a nitrogen atmosphere at a heating rate of 5 °C min^{-1}. The resulting black carbonaceous product (ZC) was used as the negative electrode material for the asymmetric supercapacitor device.

1.5. Material Characterizations

The surface morphology of the prepared materials was analysed using FE-SEM (JEOL JSM-6700F Field Emission). TEM and HR-TEM (JEOL JEM-F200) with a SAED were employed to examine the intrinsic morphology and structural properties of the materials. The information on the elemental distribution of the synthesised materials was examined by EDS mapping. Crystal structure and phase purity of the synthesised materials were investigated using a Bruker D8 Phaser X-ray diffractometer with Cu Kα radiation (λ=0.1541 nm). FT-IR spectra were evaluated within the 400-4000 cm^{-1} range using a Bruker EQUINOX5 FT-IR spectrophotometer and the conventional KBr disk method. Raman spectroscopy was employed to gain insights into the lattice dynamics of nanostructures at the molecular scale. This measurement utilised a Renishaw Raman InVia System with a 532 nm green laser. Thermogravimetric analysis (TGA) was performed using TA instrumentation, SDT Q600, under a controlled air atmosphere at a heating rate of 10 °C min^{-1} to analyse the thermal stability of materials. The operation details of some characterization items can refer to the literature.[2-4]

1.6. Electrochemical Characterizations

1.6.1. Electrodes preparation

Working electrodes were prepared using pre-cleaned stainless-steel (SS) mesh as current collector (1 cm × 1 cm), selected for its high electrical conductivity, mechanical robustness, and electrochemical stability. The electrodes were fabricated via a slurry-coating method. A homogeneous slurry was obtained by mixing the active material (80 wt%), polyvinylidene fluoride (PVDF, 10 wt%) as a binder, and acetylene black (10 wt%) as a conductive additive in N-methyl-2-pyrrolidone (NMP). The mixture was subsequently coated onto the SS mesh. The coated electrodes were dried in a vacuum oven to ensure complete solvent removal and proper adhesion.

1.6.2. Electrochemical measurements of the electrodes in three-electrode setup

Electrochemical characterisations were performed on a CHI 608 electrochemical workstation (CH Instruments, Austin, USA) in 2 M KOH electrolyte at ambient temperature. A three-electrode configuration was used, consisting of the active-material–loaded SS mesh as the working electrode (NCM, NCM-derived NCO, NCM-derived NCO@CNT, and ZC), graphite as the counter electrode, and a saturated calomel electrode (SCE) as the reference electrode. Cyclic voltammetry (CV) was conducted at scan rates from 10 to 100 mV s^{-1}. Galvanostatic charge–discharge (GCD) tests were performed at various current densities within potential windows of 0–0.4 V (positive electrode) and −1 to 0 V (negative electrode). Electrochemical impedance spectroscopy (EIS) was recorded in the frequency range of 1 Hz to 100 kHz.

1.6.3. *Fabrication of solid-state asymmetric supercapacitor (ASC) device*

After successful testing of electrodes in three-electrode setup, solid state ASC device was constructed to demonsatrate the real world application. ASC device consist of NCM-derived NCO@CNT as positive electrode and ZC as negative electrode. Cellulose filter paper was used as seperator to prevent electrical short-circuiting and worked as ionic seperator and PVA-KOH gel was utilized as electrolyte. PVA-KOH gel electrolytes are widely used in solid-state supercapacitors because they combine the mechanical stability of a polymer matrix with the ionic conductivity of an alkaline electrolyte. The PVA chains trap water and KOH, forming a quasi-solid gel. It supplies the ions for charge transport between electrodes during charging discharging. A PVA–KOH gel polymer electrolyte was prepared following a reported procedure.[5] 2 g of PVA was dissolved in 20 mL of distilled water under continuous stirring at 80 °C for 30 min to ensure complete dissolution and homogeneity of the PVA. Subsequently, 2 M KOH solution (10 mL) was then added dropwise to form a translucent PVA-KOH gel. This gel electrolyte was coated onto two working electrodes, which were assembled in a sandwich configuration with a separator placed between them. The device was then allowed to dry naturally at room temperature overnight, a crucial step that facilitates the setting of the gel, thereby solidifying the electrolyte matrix. This solid-state ASC device was further used in two electrode setups to evaluate charge storage, capacitive behaviour, operational capabilities and application in energy storage technologies.

The specific capacitance (F g^{-1}), energy density (Wh kg^{-1}), and power density (W kg^{-1}) were calculated using Eqs. 1-3, respectively.[6]

$$C = \frac{I \times \Delta t}{\Delta V \times m} \quad \text{..... (1)}$$

$$E = \frac{0.5 \times C \times \Delta V^2}{3.6} \quad \text{..... (2)}$$

$$P = \frac{E \times 3600}{\Delta t} \quad \text{..... (3)}$$

where C denotes the specific capacitance (F g^{-1}), I the discharge current (mA cm^{-2}), Δt the discharging time (s), ΔV the potential window (V), and m the mass of active material (g), E and P represent the energy density (Wh kg^{-1}) and power density (W Kg^{-1}), respectively. The active material loadings were 1.8, 1.8, and 1.5 mg for NCM, NCM-derived NCO and NCM-derived NCO@CNT electrodes, respectively.

For the construction of the ASC device, charge balance between the positive and negative electrodes is essential because of their differing specific capacitances and operating potentials. Accordingly, the mass ratio of the electrodes was adjusted to satisfy the charge balance condition, calculated using Eq. 4.[7]

$$\frac{m_+}{m_-} = \frac{C_{s-} \times \Delta V_-}{C_{s+} \times \Delta V_+} \quad \text{..... (4)}$$

Where m_+ and m_- (g cm^{-2}) denotes mass deposited, C_{s+} and C_{s-} (F g^{-1}) denotes specific capacitance, ΔV_+ and ΔV_- (V) denotes potential window of the positive electrode (NCM-derived NCO@CNT), and the negative electrode (ZC), respectively.

By calculation, the mass balancing ratio is,

$$\frac{m_+}{m_-} = 0.65$$

2. List of Figures and Captions

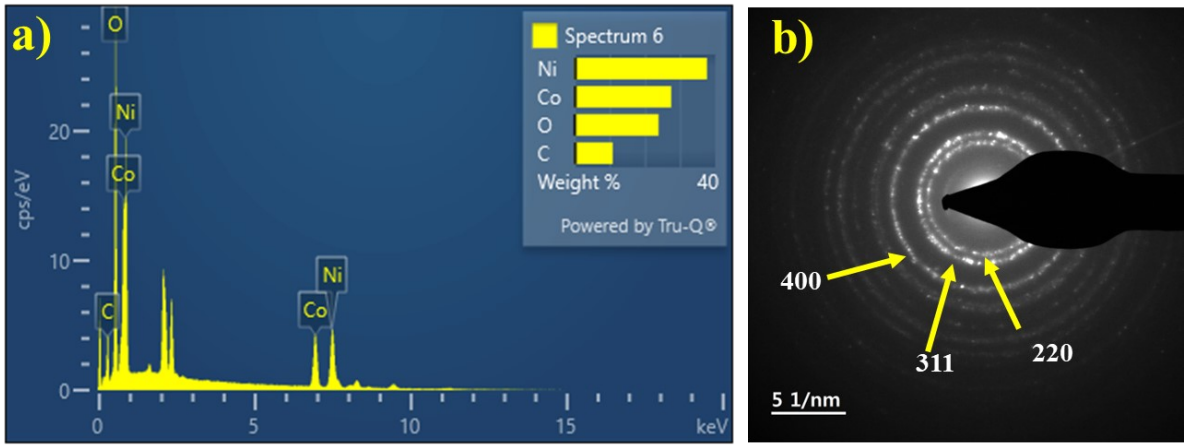

Fig. S1. (a) EDX spectrum, (b) SAED pattern of NCM-derived NCO@CNT composites.

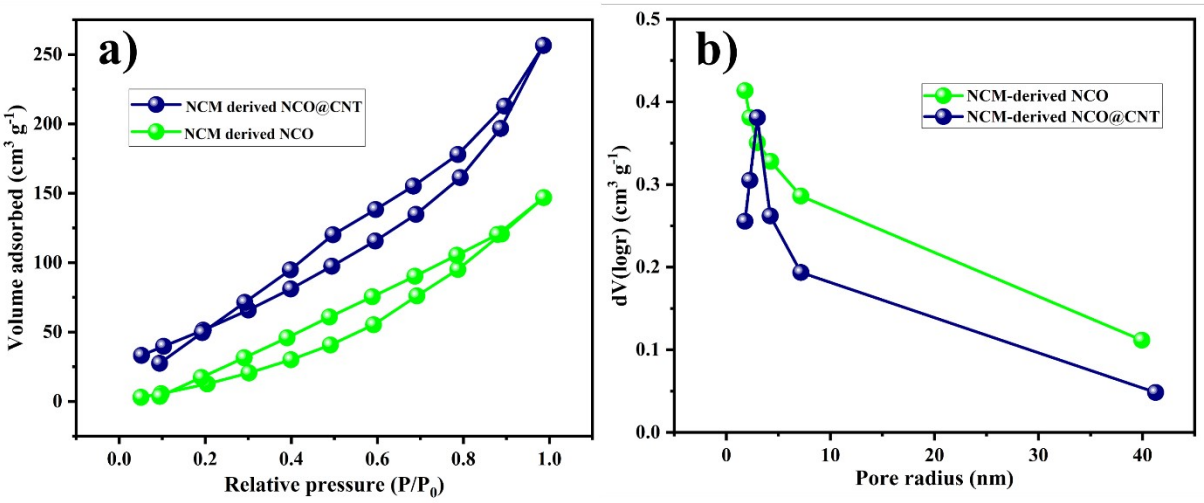

Fig. S2. (a) Nitrogen adsorption–desorption isotherm, (b) BJH pore size distribution curves of NCM-derived NCO and NCM-derived NCO@CNT composites.

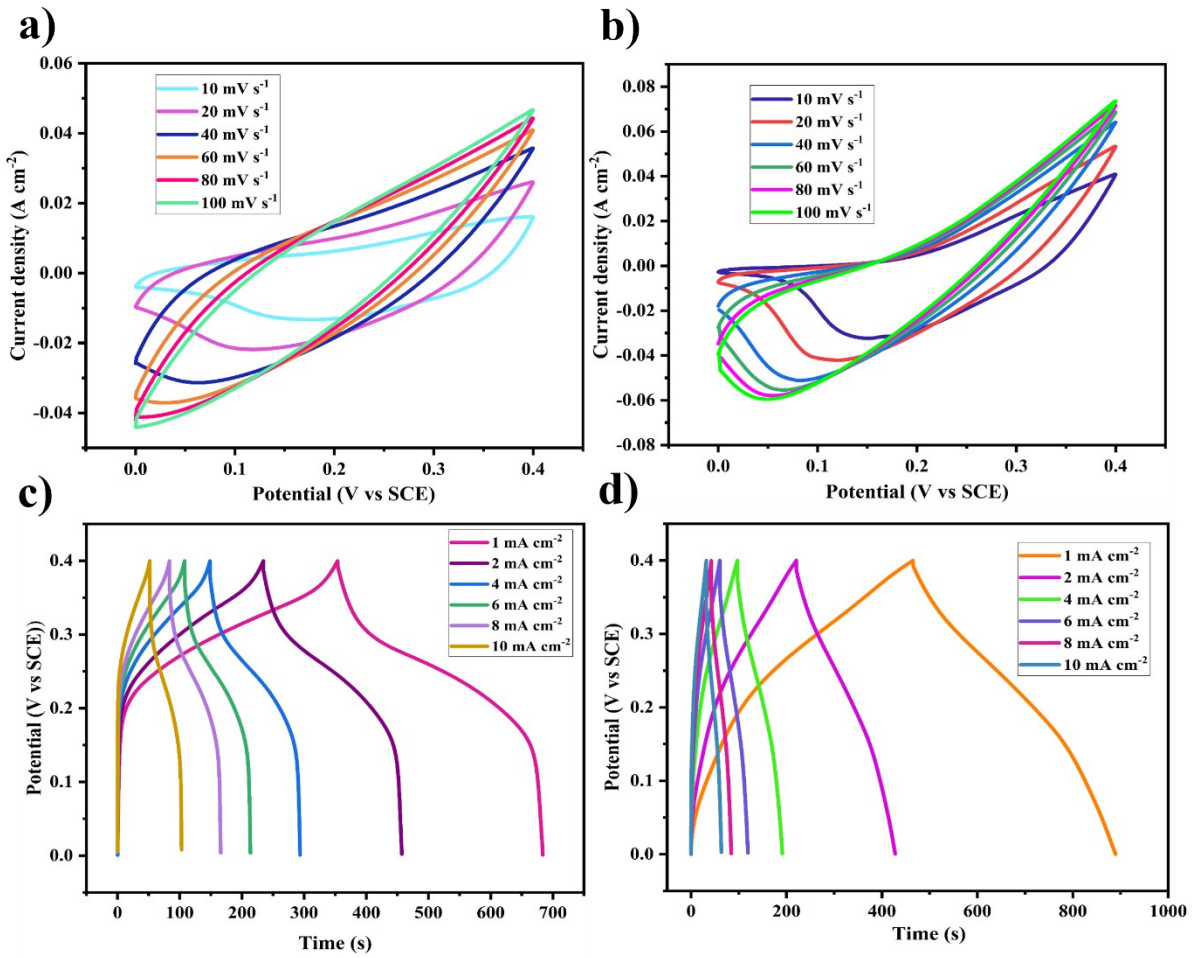

Fig. S3. (a,b) CV curves of NCM and NCM-derived NCO at scan rates ranging from 10 to 100 mV s^{-1}. (c,d) Galvanostatic charge–discharge (GCD) curves of NCM and NCM-derived NCO at current densities from 1 to 10 mA cm^{-2}.

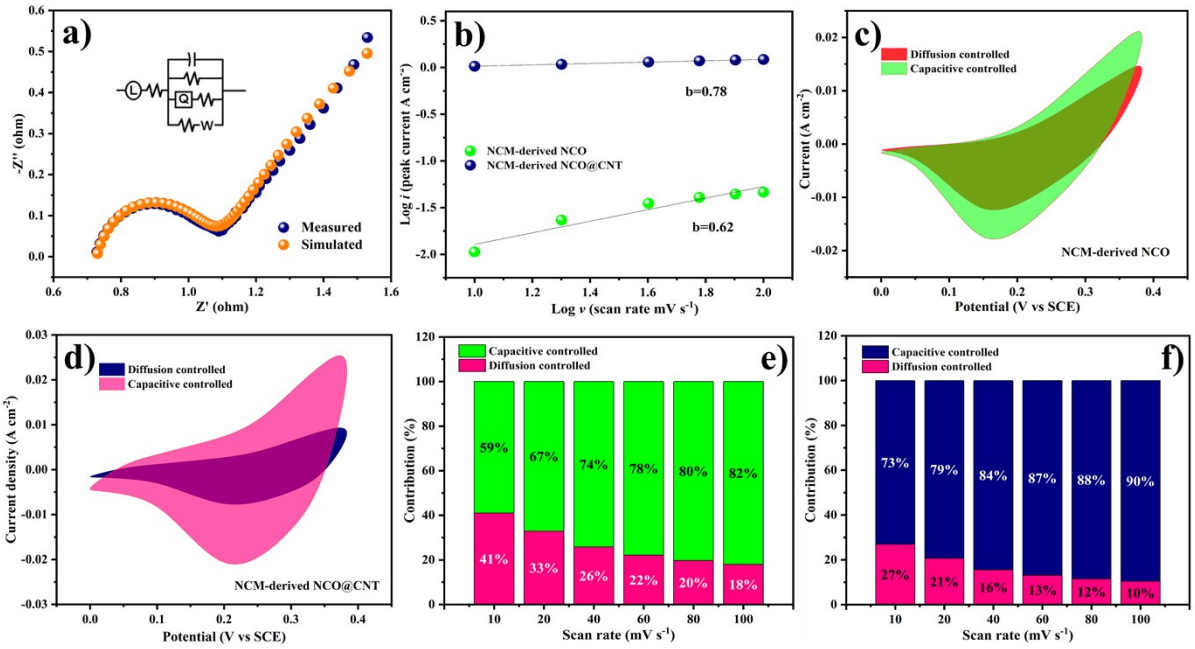

Fig. S4. (a) Simulated Nyquist plot of NCM-derived NCO@CNT (inset: equivalent circuit). (b) Log(scan rate) versus log(peak current). (c,d) CV curves showing capacitive and diffusion-controlled contributions at 10 mV s^{-1} for NCM-derived NCO and NCM-derived NCO@CNT. (e,f) Percentage contributions of capacitive and diffusion-controlled processes for NCM-derived NCO and NCM-derived NCO@CNT at various scan rates.

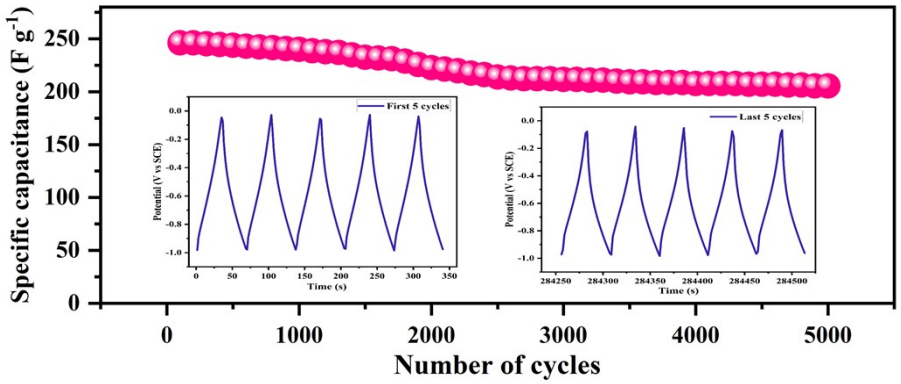

Fig. S5. Cyclic stability of ZC over 5000 charge-discharge cycles (inset: comparison of the first and last five cycles)

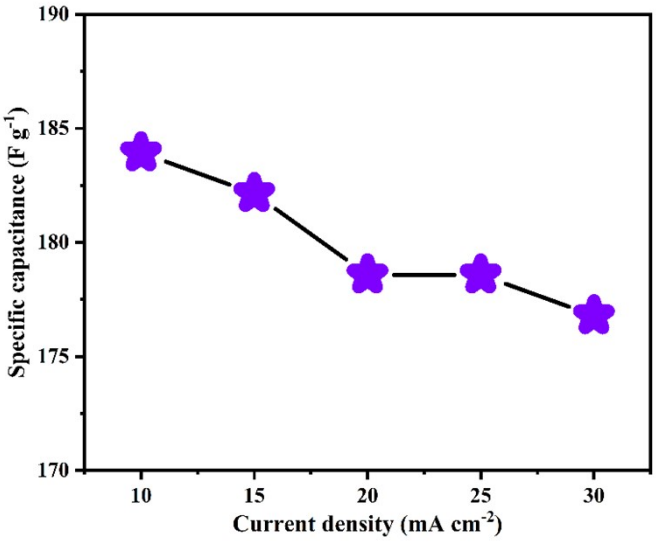

Fig. S6. Specific capacitance of the NCM-derived NCO@CNT//ZC composite at the different current densities.

Table 1. Comparison of the electrochemical performance of the NCM-derived NCO@CNT composite with previously reported supercapacitor materials.

Electrode material	Specific capacitance	Electrolyte	Device configuration	Energy density	Power density	Ref.
Ni/Co-MOF	1070 F g^{-1} at 0.5 mA cm^{-2}	1 M KOH	Ni/Co-MOF// Ni/Co-MOF	30.96 Wh kg^{-1}	3.2 W kg^{-1}	8
MOF-derived $MnFe_2O_4$	1226 F g^{-1} at 1 mA cm^{-2}	1 M Na_2SO_4	$MnFe_2$-MOF//AC	32.67 Wh kg^{-1}	1000 W kg^{-1}	9
$NiCo_2O_4$@N-MWCNT	1191 F g^{-1} at 1 A g^{-1}	1 M KOH	-	-	-	10
NiFe-LDH@CNT	1243 F g^{-1} at 1 A g^{-1}	6 M KOH	NiFe-LDH@CNT//AC	57.6 Wh kg^{-1}	1136 W kg^{-1}	11
In_2O_3/g-C_3N_4/MWCNT	1081 F g^{-1} at 1 A g^{-1}	2 M KOH	In_2O_3/g-C_3N_4/MWCNT//AC	57.5 Wh kg^{-1}	2760 W kg^{-1}	12
Mn_2O_3/GO	588 F g^{-1} at 0.5 mA cm^{-2}	1 M Na_2SO_4	EMG-5%/Li-chip	925 Wh kg^{-1}	3.3 kW kg^{-1}	13
CNT-U-CVO	244 F g^{-1} at 2 mA cm^{-2}	2 M KOH	CNT-U-CVO//AC	6.93 Wh kg^{-1}	320 W kg^{-1}	14

Cerium selenide/MWCNT	451.4 F g^{-1} at 2 mA cm^{-2}	$Na_2S_2O_3$	Cerium selenide/MWCNT//Cerium selenide/MWCNT	36.3 Wh kg^{-1}	2.8 kW kg^{-1}	15
NCM-derived NCO@CNT	1466.6 F g^{-1} at 1 mA cm^{-2}	2 M KOH	NCM-derived NCO@CNT//ZC	48.12 Wh kg^{-1}	5250 W kg^{-1}	**This work**

References

1 P. Sardar, G. Bhattacharya, R. Manna, S. Raj, S. Rahut and A. Nath Samanta, *Adv. Powder Technol.*, 2024, **35,** 104344.

2 J. Sun, M. Yan, G. Tao, R. Su, X. Xiao, Q. Wu, F. Chen, X. Wu, H. Lin, *Water Res*. 2025, **268,** 122627.

3 J. Wang, H. Wang, L. Shen, R. Li, H. Lin, *Water Res*. 2023, **244**, 120530.

4 X. Yao, R. Li, L. Shen, L. Zhao, H. Lin, *Water Res*. 2025, **287**, 124436.

5 S. B. Bandgar, M. M. Vadiyar, C. L. Jambhale, J. Kim and S. S. Kolekar, *J. Alloys Compd.,* 2021, **853**, 157129.

6 D. M. Ulisso, S. A. Mane, R. A. Chavan, G. P. Kamble, S. S. Kolekar and A. V. Ghule, *J. Alloys Compd.*, 2024, **980**, 173563.

7 D. M. Sayed, M. M. Taha, L. G. Ghanem, M. S. El-Deab and N. K. Allam, *J. Power Sources*, 2020, **480**, 229152.

8 A. A. Bhoite, V. A. Sawant and N. L. Tarwal, *Colloids Surf., A,* 2024, **702**, 134814.

9 R. Bhosale, S. Bhosale, R. Sankannavar, V. Chavan, C. Jambhale, H. Kim and S. Kolekar, *ACS Appl. Nano Mater.*, 2024, **7**, 4078–4091.

10 R. Kumar, S. Ramesh, V. Kakani and Y. Haldorai, C. Karthikeyan, B. Kumar, N. Siva Kumar, M. Asif, S. Kumar, P. Babu, K. Reddy, V. Pasupuleti, *Diamond Relat. Mater.* 2024, **141**, 110660.

11 A. C. Vittal Rao Manjunatha Rao, S. Golla, C. K. Rastogi and M. Channegowda, *ACS Appl. Electron. Mater.*, 2025, **7**, 48–63.

12 N. James and S. PB, *Electrochim. Acta*, 2024, **507**, 145192.

13 A. M. Teli, S. A. Beknalkar, V. C. Karade, S. M. Mane, J. Go, P. S. Patil and J. C. Shin, *J. Mater. Sci. Mater. Electron.*, 2022, **33**, 8844–8857.

14 S. V. Desarada, M. A. Yewale, S. Vallabhapurapu, V. S. Vallabhapurapu, S. D. Dhas, A. A. Al-Kahtani, A. B. Bhorde, V. Kumar and D. K. Shin, *Diamond Relat. Mater.*, 2024, **149,** 111557.

15 B. Pandit and B. R. Sankapal, *ACS Appl. Nano Mater.*, 2022, **5**, 3007–3017.